

Structural Changes and Thermal Stability of Charged $\text{LiNi}_x\text{Mn}_y\text{Co}_z\text{O}_2$ Cathode Materials Studied by Combined *In Situ* Time-Resolved XRD and Mass Spectroscopy

Seong-Min Bak,[†] Enyuan Hu,[†] Yongning Zhou,[†] Xiqian Yu,[†] Sanjaya D. Senanayake,[†] Sung-Jin Cho,^{*,§,∇} Kwang-Bum Kim,^{||} Kyung Yoon Chung,[‡] Xiao-Qing Yang,^{*,†} and Kyung-Wan Nam^{*,⊥}

[†]Chemistry Department, Brookhaven National Laboratory, Upton, New York 11973, United States

[‡]Center for Energy Convergence Research, Korea Institute of Science and Technology (KIST), Seoul 136-791, Republic of Korea

[§]Johnson Control Advanced Power Solution, Milwaukee, Wisconsin 53209, United States

[∇]Joint School of Nano Science & Nano Engineering, North Carolina A&T State University, Greensboro, North Carolina 27401, United States

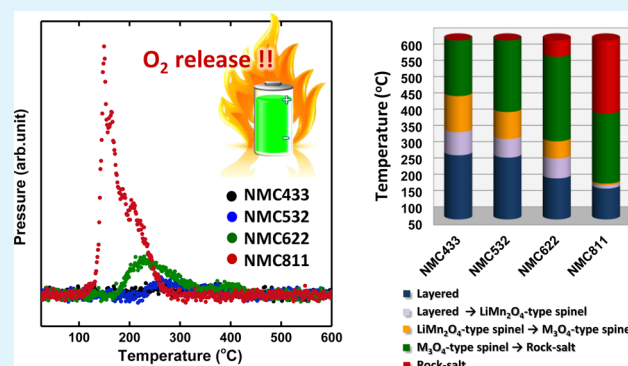
^{||}Department of Material Science and Engineering, Yonsei University, Seoul 120-749, Republic of Korea

[⊥]Department of Energy and Materials Engineering, Dongguk University, Seoul 100-715, Republic of Korea

S Supporting Information

ABSTRACT: Thermal stability of charged $\text{LiNi}_x\text{Mn}_y\text{Co}_z\text{O}_2$ (NMC, with $x + y + z = 1$, $x:y:z = 4:3:3$ (NMC433), $5:3:2$ (NMC532), $6:2:2$ (NMC622), and $8:1:1$ (NMC811)) cathode materials is systematically studied using combined *in situ* time-resolved X-ray diffraction and mass spectroscopy (TR-XRD/MS) techniques upon heating up to 600 °C. The TR-XRD/MS results indicate that the content of Ni, Co, and Mn significantly affects both the structural changes and the oxygen release features during heating: the more Ni and less Co and Mn, the lower the onset temperature of the phase transition (i.e., thermal decomposition) and the larger amount of oxygen release. Interestingly, the NMC532 seems to be the optimized composition to maintain a reasonably good thermal stability, comparable to the low-nickel-content materials (e.g., NMC333 and NMC433), while having a high capacity close to the high-nickel-content materials (e.g., NMC811 and NMC622). The origin of the thermal decomposition of NMC cathode materials was elucidated by the changes in the oxidation states of each transition metal (TM) cations (i.e., Ni, Co, and Mn) and their site preferences during thermal decomposition. It is revealed that Mn ions mainly occupy the $3a$ octahedral sites of a layered structure ($R\bar{3}m$) but Co ions prefer to migrate to the $8a$ tetrahedral sites of a spinel structure ($Fd\bar{3}m$) during the thermal decomposition. Such element-dependent cation migration plays a very important role in the thermal stability of NMC cathode materials. The reasonably good thermal stability and high capacity characteristics of the NMC532 composition is originated from the well-balanced ratio of nickel content to manganese and cobalt contents. This systematic study provides insight into the rational design of NMC-based cathode materials with a desired balance between thermal stability and high energy density.

KEYWORDS: energy storage, Li-ion battery, safety, synchrotron X-ray diffraction, layered structure



INTRODUCTION

Lithium ion batteries (LIBs) are considered to be the best candidates for powering electrified automobiles such as plug-in hybrid electric vehicles (PHEVs) and electrical vehicles (EVs). Although extensive efforts have been made on the development of LIBs, significant improvements in energy density, cycle life, and safety characteristics are still required for their successful wide deployment in automotive applications.^{1–3} The safety characteristics of the LIBs are one of the most critical barriers to be overcome, especially in large-scale automotive applications.

As one of the most promising cathode materials for the high-energy-density LIBs, the Ni-based layered cathode materials such as $\text{LiNi}_{0.8}\text{Co}_{0.15}\text{Al}_{0.05}\text{O}_2$ (NCA) and $\text{LiNi}_x\text{Mn}_y\text{Co}_z\text{O}_2$ (NMC, $x + y + z = 1$) have been extensively studied, because of its high capacity and low cost, compared with widely used LiCoO_2 commercial material.^{4–8} Recently, taking advantage of its high capacity, NCA materials have been successfully adopted

Received: September 30, 2014

Accepted: November 24, 2014

Published: November 24, 2014

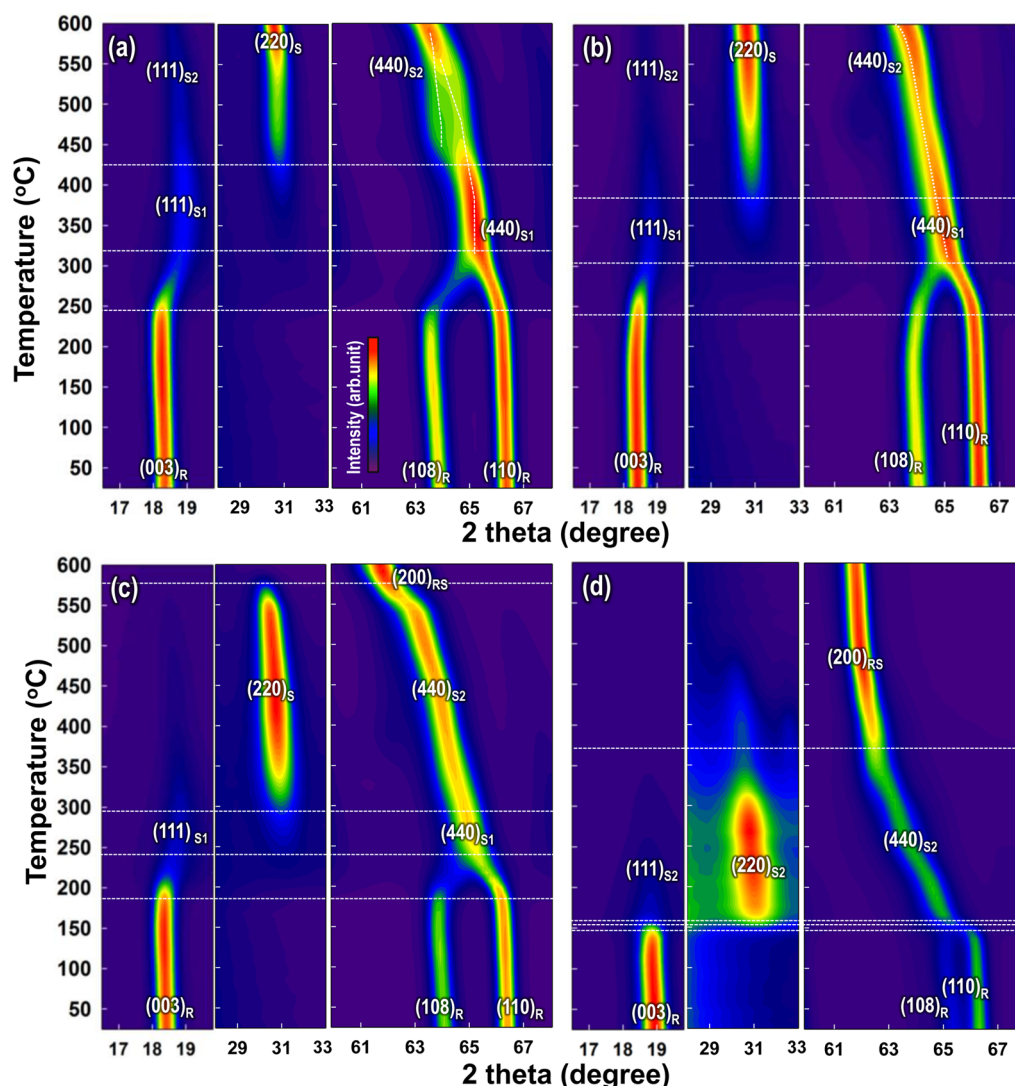


Figure 1. Contour plots of the TR-XRD patterns at the selected 2θ range for the charged (a) NMC433, (b) NMC532, (c) NMC622, and (d) NMC811.

in an all-electric vehicle launched by Tesla Motors, which uses ~ 7000 of Panasonic's cylindrical 18 650 cells in the LIB pack.^{9,10} However, despite its commercial success, the poor thermal stability of NCA cathode material, which could jeopardize the safety of the batteries, is still an important issue that needs to be addressed.¹¹ It was reported that, at highly delithiated (i.e., charged) states, the reduction of Ni^{4+} to Ni^{2+} during heating releases oxygen that can cause severe thermal runaway by reacting with the flammable electrolytes and lead to catastrophic failure of the LIBs.^{12–14} This oxygen-release-related safety concern is considered to be the main drawback to the use of Ni-rich cathode materials, despite its obvious advantage in high capacity. More thermally stable cathode materials with reduced Ni concentration (typically $\text{LiNi}_{1/3}\text{Mn}_{1/3}\text{Co}_{1/3}\text{O}_2$, NMC333) have been also developed. As one of the representative NMC layered materials, the NMC333 shows much better thermal stability than the NCA material.¹⁴ However, the higher thermal stability is achieved at the expense of the capacity (i.e., energy density). In recent years, Ni-rich NMC materials have emerged as alternatives to increase energy density, as evidenced by the fact that more and more battery manufacture companies are actively pursuing the Ni-rich NMC

chemistry in their applications for PHEVs and EVs. As reported in the literature, for the Ni-based layered cathode systems, both the charge–discharge capacity and the thermal stability is strongly dependent on the contents of nickel, cobalt, and manganese in the structure.^{15–19} For example, it is well-known that a high nickel content contributes to a higher capacity at the expense of the safety characteristics, while high cobalt and manganese content improves the cycling and safety characteristics at the expense of the capacity.^{15–18,20} Therefore, compositional optimization of the NMC chemistry is quite important for improving the electrochemical performance and safety characteristics of LIBs using cathode materials based on the NMC chemistry.

Therefore, the systematic investigation of thermal stability on a series of NMC cathode materials with different compositions will undoubtedly provide important information on formulating high capacity materials with reasonably good safety characteristics. Unfortunately, not much systematic studies on the thermal stability characteristics of the full series of NMC cathode chemistries have been reported so far. In our previous publication, an *in situ* technique that combined time-resolved X-ray diffraction and mass spectroscopy (TR-XRD/MS) to

simultaneously monitor the structural changes and the released gas species (including O₂ and CO₂) during the thermal decomposition of charged NCA cathode materials was reported.²¹ In this paper, we report systematic studies on the thermal stability of a series of charged LiNi_xMn_yCo_zO₂ cathode materials ($x:y:z = 4:3:3, 5:3:2, 6:2:2, 8:1:1$, and $x + y + z = 1$), using this combined TR-XRD and MS technique. We show that these charged materials undergo a specific path of phase transitions (i.e., thermal decomposition)—from layered (space group $R\bar{3}m$) to spinel (space group $Fd\bar{3}m$), and then to rock-salt (space group $Fm\bar{3}m$)—as a function of heating temperature, which correlates with the evolution of oxygen. Through the comparison of the TR-XRD/MS results for each composition of NMC cathodes, it is revealed that NMC532 is an optimized composition that has good thermal stability, comparable to the low-nickel-content materials (e.g., NMC333 and NMC433) while still maintaining a high capacity, close to that of the high-nickel-content materials (e.g., NMC811 and NMC622). This study will serve as a good guide to the rational design of the NMC cathode materials for desired performance and safety characteristics and the development of new cathode materials.

EXPERIMENTAL SECTION

A series of LiNi_xMn_yCo_zO₂ cathode materials (NMC with $x + y + z = 1$, $x:y:z = 4:3:3$ (NMC433), $5:3:2$ (NMC532), $6:2:2$ (NMC622), and $8:1:1$ (NMC811)) were obtained from an industrial partner. The NMC cathode materials used in this study are bare, without any surface modifications. The cathode electrodes were prepared from a mixed slurry of 80 wt% active material, 10 wt% carbon black (Chevron), and 10 wt% PVDF (Kureha) binder in an *n*-methyl pyrrolidone (NMP) solvent. The slurry was subsequently coated onto an aluminum foil. The cathode electrodes were incorporated into 2032 coin cells with a Li metal foil anode, a Celgard separator, and an electrolyte of 1.2 M LiPF₆ dissolved in ethylene carbonate (EC) and dimethyl carbonate (DMC) solvent (3:7 by volume). The coin cells were charged to 4.3 V, using a constant current (i.e., galvanostatic) with a C/30 rate. The lithium contents of each sample, after charging to 4.3 V, were estimated by the charge passed in the cell, assuming 100% coulombic efficiency. Thus, the real composition of the charged samples used in this work for NMC433, NMC532, NMC622, and NMC 811 are estimated as Li_{0.34}Ni_{0.4}Mn_{0.3}Co_{0.3}O₂, Li_{0.29}Ni_{0.5}Mn_{0.3}Co_{0.2}O₂, Li_{0.27}Ni_{0.6}Mn_{0.2}Co_{0.2}O₂, and Li_{0.22}Ni_{0.8}Mn_{0.1}Co_{0.1}O₂, respectively. Constant current charge curves are presented at Figure S1 in the Supporting Information. The charged cells were then transferred to an argon-filled glovebox for disassembly. The charged cathodes were thoroughly washed using DMC solvent to eliminate residual salts and then gently scraped from the current collector (aluminum foil) as samples for the TR-XRD/MS measurements.

The TR-XRD data were collected at beamline X7B ($\lambda = 0.3196$ Å) of the National Synchrotron Light Source (NSLS), using an image plate detector in transmission mode. Approximately 3.5–4.0 mg of the charged cathode sample was loaded into a quartz capillary with an inner diameter of 0.7 mm and two open ends. One end of the capillary was connected to the helium carrier gas and the other end was connected to a residual gas analyzer mass spectrometer (Model RGA200, Stanford Research Systems) with a flow meter to detect gas species released from the sample during heating. Quartz wool was placed on each side of the sample to prevent movement of sample due to the helium carrier gas flow. TR-XRD patterns (~4 min for each XRD scan) and MS signal were simultaneously collected in a continuous manner as the sample was heated from room temperature to 600 °C for 4 h (i.e., at a heating rate of ~2.4 °C min⁻¹). The XRD patterns of selected samples were refined by Le Bail methods, using the GSAS package with the EXPGUI interface.²²

The Ni and Co K-edge X-ray absorption near-edge structure (XANES) spectra were collected at the 1D-XRS-KIST beamline of the Pohang Accelerator Laboratory (PAL) in transmission mode. Reference spectra of Ni and Co metallic foils were collected simultaneously with all of the spectra for energy calibration.

RESULTS AND DISCUSSION

Figures 1a–d presents contour plots of the TR-XRD patterns at the selected 2θ angle range for the Li_{0.34}Ni_{0.4}Mn_{0.3}Co_{0.3}O₂ (NMC433), Li_{0.29}Ni_{0.5}Mn_{0.3}Co_{0.2}O₂ (NMC532), Li_{0.27}Ni_{0.6}Mn_{0.2}Co_{0.2}O₂ (NMC622), and Li_{0.22}Ni_{0.8}Mn_{0.1}Co_{0.1}O₂ (NMC811), respectively. The original TR-XRD patterns are also provided in Figure S2 in the Supporting Information. The refinement of room-temperature XRD for each sample using Le Bail methods (Figure S3 in the Supporting Information) showed that the initial layered structure of rhombohedral symmetry ($R\bar{3}m$) was preserved after charging to 4.3 V. During the course of heating, all of the NMC samples showed a similar route of structural change from the layered ($R\bar{3}m$) to disordered spinel (LiMn₂O₄-type, $Fd\bar{3}m$) structure as the first stage of thermal decomposition. The coalescence of the (108)_R and (110)_R peaks and disappearance of (003)_R peak in the layered structure indicate the onset of the phase transition to the disordered spinel phase.^{23–25} As shown in Figures 1a–d, the onset temperature for the first phase transition from a layered structure to a disordered spinel structure is strongly dependent on the nickel, cobalt, and manganese contents.

As shown in Figure 1a, the NMC433 with lowest nickel content among the four samples started the first phase transition from the layer structure to the disordered LiMn₂O₄-type spinel (called “S1” in this paper) at 245 °C and completed at ~325 °C with a temperature range spanning ~80 °C. At a higher temperature range (~450 °C), a clear indication of a new spinel phase formation can be observed through the appearance of a (220)_S peak, as shown in Figure 1a. This new peak grew stronger and stronger with increasing temperature and remained strong to the terminating temperature at 600 °C in our experiments. This new spinel phase (denoted as “S2” in this work) is not the same as the LiMn₂O₄-type spinel (denoted as S1) observed in the low-temperature region. It is assigned as M₃O₄-type spinel (e.g., Co₃O₄, JCPDS File Card No. 43-1003) with the same $Fd\bar{3}m$ space group. The major differences of these two types of spinels are the different lattice parameters and cation occupations, in particular, at the 8a tetrahedral sites of the spinel structure.^{26–28} The formation and growth of M₃O₄-type spinel can be indicated by the appearance and growth of the (220)_S XRD peak shown in Figure 1a. Because the (220)_S peak can be observed only if partial (or total) occupancy of the transition metals (TMs) (e.g., Ni, Co, and Mn) in the 8a tetrahedral sites, which are only occupied by the Li ions in S1 spinel, has occurred. The intensity of this peak is proportional to the amount of TM cations migrated into these 8a tetrahedral sites. If a significant amount of TM cations occupy these tetrahedral 8a sites, the structure is the M₃O₄-type spinel (e.g., [Co²⁺]_{tet}[2Co³⁺]_{oct}O₄ (Co₃O₄) if M = Co). We have also carried out a profile matching of the XRD pattern of the NMC433 collected at 500 °C with two types of spinel phases. This two-phase fitting gave us a satisfactory result, further confirming the co-existence of two spinel phases with different lattice parameters (see Figure S4 in the Supporting Information). This M₃O₄-type spinel structure differs from the LiMn₂O₄-type spinel structure, where

most of the tetrahedral sites are occupied by Li only. It has been reported that the formation of the M_3O_4 -type spinel structure pushes the phase transition (i.e., thermal decomposition) to the rock-salt structure to a higher temperature, resulting in improved thermal stability.²⁷ No clear indications of the MO-type rock-salt phase formation, which should be indicated by the growth of $(200)_{RS}$ and disappearance of $(111)_S$ peaks, were observed for this NMC433 sample up to 600 °C.

When the nickel content is increased slightly, in the case of the NMC532 (Figure 1b), the first phase transition from layered to disordered $LiMn_2O_4$ -type spinel structure started at ca. 235 °C and was completed at ca. 315 °C; both temperatures are ~ 10 °C lower than those of the NMC433 sample. The $Fd\bar{3}m$ symmetry was preserved up to 600 °C, just like in the NMC433 case. The first phase transition for NMC532 occurred at a slightly lower temperature than in the NMC433 case, indicating a slightly poorer thermal stability than the NMC433. However, note that the formation of a M_3O_4 -type spinel started at ~ 400 °C in the NMC532 sample, which is lower than the 450 °C for NMC433 sample (see Figure 1b). This suggests that the amount of TM cation migration (mostly Co) to the 8a tetrahedral sites during heating in NMC532 sample is less than NMC433 sample, where the Co:Ni ratio is higher.

For the NMC622 sample (Figure 1c), which is considered to be a Ni-rich material, the phase transitions (i.e., thermal decomposition) started at considerably lower temperatures and completed over much narrower temperature ranges for both the $LiMn_2O_4$ and M_3O_4 -type spinel phases, in comparison with those observed for the NMC433 and NMC532 samples. The first phase transition started at ca. 185 °C and completed at ca. 245 °C. This is followed by the formation, growth, and finally disappearance of M_3O_4 -type spinel in the temperature range of 310–550 °C; at ~ 550 °C, the phase transition from M_3O_4 -type spinel to the rock-salt structure is completed. In contrast to the NMC433 and NMC532 cases, the NMC622 completely transformed to the rock-salt phase before the end of the heating to 600 °C, indicated by the total disappearance of $(111)_S$ and $(220)_S$ peaks, together with the strengthening and sharpening of the $(200)_{RS}$ peak.

In the case of the NMC811 sample, which has the highest nickel content in this work, as shown in Figure 1d, all the phase transitions were initiated at the lowest temperatures, and the temperature range of the existence of M_3O_4 -type spinel phase is the smallest, compared to that of the other three NMC samples. The first phase transition started at ca. 135 °C and the second phase transition, from S1 to S2, was completed at ca. 155 °C, over a very narrow temperature range (~ 20 °C). This is followed by the third phase transition from disordered spinel to rock-salt, which is completed at ca. 365 °C. At the high temperature region above 365 °C, the major parts of the NMC811 sample remained in the rock-salt structure and a small part of the NMC811 sample even reduced all the way to the metallic Ni phase at the end of heating (as indicated by the XRD peaks marked in Figure S2 in the Supporting Information).

Comparing the diffraction patterns in Figure 1, we can clearly see the effects of the Co:Ni ratio on the thermal structural stability. For NMC422 and NMC532 samples with higher Co:Ni ratios, the phase transition to both S1 and S2 spinels occurred at higher temperatures and the S2 spinel remained as the dominating phase all the way up to 600 °C. In contrast, for the NMC622 and NMC811 samples with lower Co:Ni ratios,

the phase transitions to both S1 and S2 occurred and were completed at much lower temperatures, and the phase transition to rock-salt phase was completed at 550 and 365 °C, respectively. These Co:Ni-ratio-dependent structural changes are mainly due to the preferred occupancy of Co^{2+} at the tetrahedral 8a sites, making the S2 spinel stable at higher temperatures and pushed the phase transition to the rock-salt structure to higher temperatures. It is also worthwhile to point out the big decrease in thermal stability from NMC532 to NMC622, indicating that the critical high nickel content should be limited to NMC532.

The MS profiles for the oxygen (O_2 , $m/z = 32$), which were collected simultaneously during measurement of TR-XRD data for the four samples, are plotted in Figure 2. The lower panel

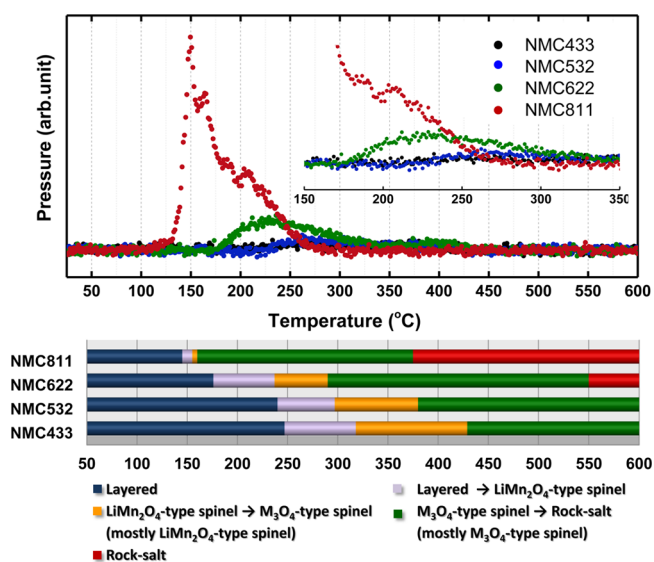
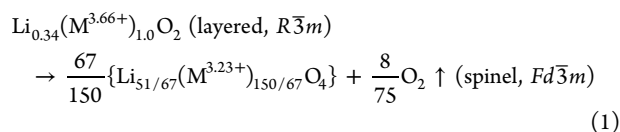


Figure 2. Mass spectroscopy profiles for the oxygen (O_2 , $m/z = 32$) collected simultaneously during measurement of TR-XRD and the corresponding temperature region of the phase transitions for NMC samples (lower panel).

presents reference guide lines for the temperature ranges of phase transitions for the four charged NMC433, NMC532, NMC622, and NMC811 samples based on the TR-XRD results in Figure 1. It is clearly shown that the oxygen evolution peaks coincide well with the phase transitions for these samples. For the NMC433, no clear O_2 release peak was observed, which indicates good thermal stability of the NMC433 material. It should be noted that this lack of oxygen release peak does not necessarily mean “no evolution” of oxygen. In the NMC cathode materials, Ni^{2+} and Co^{3+} are the electrochemically active ions and the charge compensation during lithium extraction (i.e., charging) must be accompanied by the oxidation of Ni^{2+} to Ni^{3+} and Ni^{4+} , and Co^{3+} to Co^{4+} , respectively.^{17,27,29,30} The average oxidation states of Ni and Co for the series of NMC samples before and after charging were confirmed by X-ray absorption near edge structure (XANES) spectroscopy (see Figure S5 in the Supporting Information). Since the Ni^{3+} and Ni^{4+} ions would be reduced to Ni^{2+} ions upon heating, the oxygen release from the structure is inevitable, to maintain the overall charge neutrality. For example, in the case of charged NMC 433 (i.e., $Li_{0.34}Ni_{0.4}Mn_{0.3}Co_{0.3}O_2$), the oxygen release occurs via the following reaction (eq 1):^{21,31}



where “layered” = LiMO_2 and “spinel” = $(\text{Li}+\text{M})_3\text{O}_4$.

Therefore, in the case of NMC433 sample, it is more likely that the oxygen release in very small amounts spreads in a wide temperature range. For the NMC532 sample, the oxygen release behavior is quite similar to that of the NMC433 sample. This might be due to the just slightly higher nickel content in the NMC532 than in the NMC433.

In the charged NMC622 sample with increased nickel content and decreased cobalt and manganese contents, oxygen release becomes much more pronounced and a significant peak was observed, as shown in Figure 2. For the charged NMC811, the rapid structural changes resulted in a very sharp O_2 release peak with a maximum at $\sim 150^\circ\text{C}$. This substantial O_2 release starts at ca. 130°C , which coincides well with the onset temperature of the first phase transition from layered phase to spinel phase. This is in sharp contrast to the small O_2 release over the wide temperature range for the low-nickel-content NMC cathodes, such as NMC433 and NMC532. Even though the thermal stability of charged NMC cathodes materials in this study was investigated without the presence of electrolytes, the results obtained in this work are highly relevant to the safety issues of real battery system. The sharp O_2 release at low temperatures, especially for the high-nickel-content NMC811 cathode, would cause serious safety problems for the LIB cell. In a real LIB cell, where a large amount of highly reactive electrolyte is available, the pulse of highly active oxygen species released from the cathode might react quickly with the flammable electrolyte and accelerate the thermal runaway.²¹ Based on the TR-XRD and MS results, the thermal stability dramatically deteriorated when the composition changed from NMC532 to NMC622, making the NMC532 a critical composition to maintain comparably good thermal stability to the NMC433 cathode materials.

Figure 3 is a schematic illustration depicting the phase stability map of the series of charged NMC materials during heating obtained from the TR-XRD results in Figure 1. As expected, the results show that the thermal stability of the charged NMC samples decreases with increasing nickel content and decreasing cobalt and manganese contents. Although this

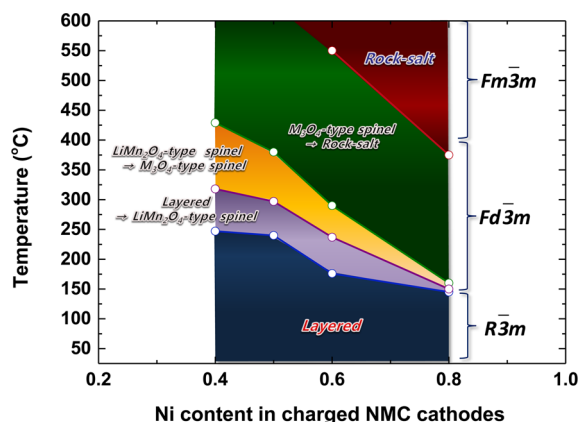


Figure 3. Schematic illustration depicting the phase stability map of the charged NMC cathode materials during heating.

trend seems straightforward, as it already has been reported in previous studies, there are some new insights that can be derived from this study about the thermal decomposition mechanism for the NMC cathode materials. There are two interesting features in Figure 3: (i) the composition-dependent starting temperature of the first phase transition ($R\bar{3}m \rightarrow Fd\bar{3}m$), which is closely related to the onset temperatures of the oxygen release for each sample, and (ii) the temperature range for the LiMn_2O_4 -type spinel and Mn_3O_4 -type spinel for each sample, which is closely related to the spreading temperature range of the oxygen release. The higher the nickel content, the lower the onset temperature of oxygen release, and the narrower the oxygen release temperature range (in other words, the poorer the thermal stability). These relationships can be explained by the different TM cation migration behaviors during heating the NMC samples discussed in the following section.

Figure 4 shows the schematic illustration of phase transitions and the possible TM cation migration paths in the charged NMC cathode materials during thermal decomposition. In the initial layered structure (Figure 4a), the TM cations occupy octahedral sites (TM_{oct} layer) and the Li^+ ions occupy the alternate layers of octahedral sites (Li_{oct} layer).²⁴ For the first phase transition from the layered to the disordered spinel, some of TM cations need to migrate from their original sites (labeled “A” in Figure 4b) to the octahedral sites in the Li layer (labeled “B” in Figure 4b). This migration will take place through a nearest tetrahedral site via the face-shared neighboring octahedra. It is well-known that this tetrahedral pathway of O_h (the octahedral site in TM layer)– T_d (tetrahedral site)– O_h (octahedral site in Li layer) is energetically favorable, because of its lower energy barrier.^{31–33} This must be accompanied by the displacement of Li^+ ions from their original sites to the adjacent tetrahedral sites to complete this first phase transition to the LiMn_2O_4 -type spinel structure, as shown in Figure 4c. As described in our previous publication,²¹ such a structure change is accompanied by the reduction of TM cations and oxygen release, if the cathode is deeply overcharged. In another of our previous studies on the thermal stability of charged NMC333 and NCA cathodes, it was reported that nickel is the most unstable element during heating for the reduction of Ni^{4+} to Ni^{2+} , followed by the reduction of Co^{3+} to Co^{2+} , while Mn is the most thermally stable element and remains close to its original state of Mn^{4+} , up to a high temperature of 400°C .²⁷ Therefore, the amount of unstable Ni^{4+} cations in the NMC structure at the charged state is the most important factor governing the thermal stability of the material. When the NMC cathode is charged to 4.3 V, most of Ni cations are oxidized to unstable Ni^{4+} ions, which will be subsequently reduced back to Ni^{3+} and then Ni^{2+} upon heating, with a concurrent loss of oxygen. During the course of this reduction process, Ni cations migrate from octahedral sites in the TM layer to octahedral sites in the Li layer. Ni cations might temporarily pass through tetrahedral sites, but they unlikely occupy these sites, since Ni cations at tetrahedral sites are not energetically stable.^{21,33} Therefore, Ni cations will migrate into and occupy the octahedral sites in the Li layer and initiate the first phase transition to the S1 type spinel when the phase transition temperature is reached.

For the Ni-rich sample such as NMC 811, the amount of unstable Ni^{4+} is larger than that of the low-nickel-content samples (e.g., NMC 433 and NMC 532) in the charged state. Since $\sim 80\%$ of the TM_{oct} layer is occupied by Ni in NMC811,

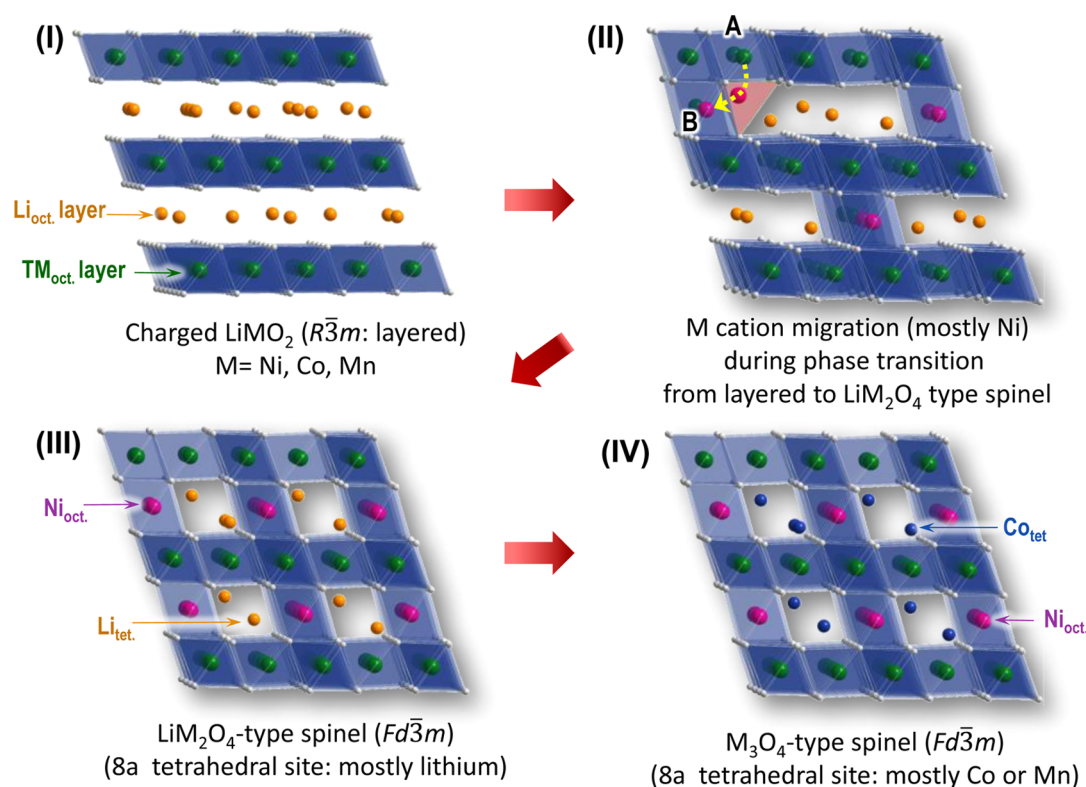


Figure 4. Schematic illustration of phase transition and the possible TM cation migration path in the charged NMC cathode materials during thermal decomposition.

it is anticipated that the Ni cation migration in NMC811 makes a greater impact on the structure changes, compared to the low-nickel-content samples, such as NMC433 and NMC532, and significantly pulled down the starting temperature of the first phase transition. Vigorous Ni cation migration from the TM_{oct} layer to the Li_{oct} layer for the NMC811 sample leads to the rapid structural changes from layered to disordered spinel driven by the rapid reduction of Ni^{4+} to Ni^{2+} , which is very consistent with the observation of rapid oxygen release during heating. In addition, the large amount of released oxygen would create a significant number of oxygen vacancies, thereby lowering the activation barrier for the migration of TM cations, and eventually accelerating the phase transitions (i.e., thermal decomposition).

While Ni cation migration starting at low temperatures is the key factor determining the onset temperature for oxygen release, the Co and Mn cation migrations occurring at higher temperatures are critical factors for the extension of the temperature range for oxygen release. The activation barrier for the Co and Mn migration is much higher than the Ni in the MO_2 framework.³³ Previous studies using first-principles calculation³³ and XAS characterization²⁷ demonstrated that the activation barrier of Mn migration is higher than that of Co, which is higher than Ni; thus, the Co migration follows the Ni migration. Since the Mn^{4+} is stable at octahedral coordination in MO_2 framework, Mn is the element most responsible for the good thermal stability of a series of NMC materials. On the other hand, we would like to point out the new finding about the important role of Co migration behavior in expanding the temperature range of oxygen release through the formation of an M_3O_4 -type spinel. As shown in Figure 4d, with further increases in temperature, the LiMn_2O_4 -type spinel structure undergoes another phase transition to M_3O_4 -type spinel

structure with an increased partial TM occupancy at the 8a tetrahedral sites. Considering the electronic configuration of Co^{2+} as $[\text{Ar}]3d^7(e^4t_2^3)$, it can be stabilized in a tetrahedral coordination, while the Ni^{2+} with an electronic configuration of $[\text{Ar}]3d^8(t_2g^6e_g^2)$ has a strong preference for the octahedral coordination. Previous studies for the NCA materials using combined TR-XRD and XAS revealed that Co ions can occupy tetrahedral sites during the phase transition from a layered structure to a spinel structure, thus forming the Co_3O_4 -type spinel phase.²¹ As mentioned above, Mn^{4+} ions are stable at octahedral coordination and are most unlikely to migrate into tetrahedral sites. Therefore, the phase transition from LiMn_2O_4 -type spinel to M_3O_4 -type spinel is strongly dependent on the Co cation migration into the 8a tetrahedral sites. Since the 8a tetrahedral sites are partially occupied by Li^+ in LiMn_2O_4 -type spinel, the kinetics of cation migration during this phase transition might be highly dependent on the Li concentration in 8a tetrahedral sites. Indeed, the charged NMC811, which contains the least lithium content in the layered structure (estimated by the charge capacity), apparently showed a direct phase transition from the layered- to M_3O_4 -type spinel structure at lower temperatures without the formation of LiMn_2O_4 -type spinel, which implies that the Co cation migration into 8a tetrahedral site readily occurred in a very short period of time. In addition, the lower cobalt content in the NMC622 and NMC811 clearly narrowed the temperature range for the thermally stable M_3O_4 -type spinel phase, making the phase transition to rock-salt structure occur at much lower temperatures, compared to the NMC433 and NMC532 with higher cobalt contents. As can be seen in Figure 2, the combined temperature range of both LiMn_2O_4 and M_3O_4 -type spinels matched reasonably well with the extended temperature range of the oxygen release for each sample, showing the higher

the cobalt content, the wider the temperature range. Therefore, when a higher fraction of cations stabilized at the tetrahedral sites, the improved thermal stability could be obtained by impeding further thermal decomposition to the rock-salt MO phase and widening the oxygen release temperature range. Based on the discussion regarding the role of each element in the NMC cathode materials during thermal decomposition (i.e., phase transitions), the reasonably good thermal stability and high capacity characteristics of the NMC532 composition could be originated from the well-balanced ratio of Ni to Mn and Co.

CONCLUSION

Thermal stability of a series of charged NMC433, NMC532, NMC622, and NMC811 cathode materials has been systematically investigated, using a combination of *in situ* TR-XRD and MS upon heating up to 600 °C. The TR-XRD/MS result clearly revealed that thermal stability of the charged NMC samples decreases with increasing nickel content but increases with increasing cobalt and manganese content: the more nickel in the sample, the lower the onset temperature of the phase transition (i.e., thermal decomposition), and the sharper the peak of the oxygen release. Since nickel is the least stable element with the largest and fastest reduction from Ni⁴⁺ to Ni²⁺ during thermal decomposition, the amount of unstable Ni⁴⁺ ions after charging to 4.3 V is the most important factor governing the thermal stability of NMC cathode materials. In contrast, Mn is the most thermally stable element, which can improve thermal stability. Co also plays an important role in maintaining good thermal stability, through extending the combined temperature range of LiMn₂O₄- and M₃O₄-type spinel phases, which is responsible for extending the temperature range of oxygen release, as observed in NMC433 and NMC532. Based on the TR-XRD and MS results, the thermal stability dramatically deteriorated from the NMC532 sample to the NMC622 sample, which makes the NMC532 sample the optimal composition for having comparably good thermal stability to the low-nickel-content materials (e.g., NMC333 and NMC433) while maintaining a high capacity that is close to the high-nickel-content materials (e.g., NMC811 and NMC622). This reasonably good thermal stability, and the high capacity characteristics, of the NMC532 composition could be due to the well-balanced ratio of nickel to manganese and cobalt. The information gained in this study will be valuable in guiding engineers and scientists to the rational design of thermally stable cathode materials with high capacity for practical LIB systems.

ASSOCIATED CONTENT

Supporting Information

Constant current charge profiles, full range ($12^\circ \leq 2\theta \leq 80^\circ$) of TR-XRD patterns for charged LiNi_xMn_yCo_zO₂, Le Bail fitting of the diffraction patterns for as-prepared LiNi_xMn_yCo_zO₂ samples after charging to 4.3 V and for the NMC433 at 500 °C. This material is available free of charge via the Internet at <http://pubs.acs.org/>.

AUTHOR INFORMATION

Corresponding Authors

*E-mail: scho1@ncat.edu (S. J. Cho).

*E-mail: xyang@bnl.gov (X.-Q. Yang).

*E-mail: knam@dongguk.edu (K.-W. Nam).

Notes

The authors declare no competing financial interest.

ACKNOWLEDGMENTS

The work at Brookhaven National Laboratory was supported by the U.S. Department of Energy, the Assistant Secretary Energy Efficiency and Renewable Energy, Office of Vehicle Technologies (under Contract No. DEAC02-98CH10886). The authors acknowledge technical support by the beamline scientists at X7B of NSLS. This work was also supported by the KIST Institutional Program (Project No. 2V03693). K.-W. Nam was supported by the Dongguk University Research Fund of 2014.

REFERENCES

- (1) Armand, M.; Tarascon, J. M. Building Better Batteries. *Nature* **2008**, *451*, 652–657.
- (2) Goodenough, J. B.; Kim, Y. Challenges for Rechargeable Li Batteries. *Chem. Mater.* **2010**, *22*, 587–603.
- (3) Thackeray, M. M.; Wolverton, C.; Isaacs, E. D. Electrical Energy Storage for Transportation—Approaching the Limits of, and Going Beyond, Lithium-ion Batteries. *Energy Environ. Sci.* **2012**, *5*, 7854–7863.
- (4) Weaving, J. S.; Coowar, F.; Teagle, D. A.; Cullen, J.; Dass, V.; Bindin, P.; Green, R.; Macklin, W. J. Development of High Energy Density Li-ion Batteries based on LiNi_{1-x-y}Co_xAl_yO₂. *J. Power Sources* **2001**, *97–8*, 733–735.
- (5) Lee, K. K.; Yoon, W. S.; Kim, K. B.; Lee, K. Y.; Hong, S. T. Characterization of LiNi_{0.85}Co_{0.10}Mn_{0.05}O₂ (M = Al, Fe) as a Cathode Material for Lithium Secondary Batteries. *J. Power Sources* **2001**, *97–8*, 308–312.
- (6) Cao, H.; Xia, B. J.; Xu, N. X.; Zhang, C. F. Structural and Electrochemical Characteristics of Co and Al Co-doped Lithium Nickelate Cathode Materials for Lithium-ion Batteries. *J. Alloys Compd.* **2004**, *376*, 282–286.
- (7) Yabuuchi, N.; Ohzuku, T. Novel Lithium Insertion Material of LiCo_{1/3}Ni_{1/3}Mn_{1/3}O₂ for Advanced Lithium-Ion Batteries. *J. Power Sources* **2003**, *119*, 171–174.
- (8) Wang, Y. D.; Jiang, J. W.; Dahn, J. R. The Reactivity of Delithiated LiNi_{1/3}Co_{1/3}Mn_{1/3}O₂, LiNi_{0.8}Co_{0.15}Al_{0.05}O₂ or LiCoO₂ with Non-Aqueous Electrolyte. *Electrochem. Commun.* **2007**, *9*, 2534–2540.
- (9) Martin, C. Driving Change in the Battery Industry. *Nat. Nanotechnol.* **2014**, *9*, 327–328.
- (10) Trippe, A.; Massier, T.; Hamacher, T. Optimized Charging of Electric Vehicles with Regard to Battery Constraints—Case Study: Singaporean Car Park. In *Energytech*; May 21–23 2013; IEEE: Piscataway, NJ, 2013; pp 1–6.
- (11) Kim, T. H.; Park, J. S.; Chang, S. K.; Choi, S.; Ryu, J. H.; Song, H. K. The Current Move of Lithium Ion Batteries Towards the Next Phase. *Adv. Energy Mater.* **2012**, *2*, 860–872.
- (12) Belharouak, I.; Lu, W. Q.; Vissers, D.; Amine, K. Safety Characteristics of LiNi_{0.8}Co_{0.15}Al_{0.05}O₂ and LiNi_{1/3}Co_{1/3}Mn_{1/3}O₂. *Electrochem. Commun.* **2006**, *8*, 329–335.
- (13) Dahn, J. R.; Fuller, E. W.; Obrovac, M.; Vonsacken, U. Thermal Stability of Li_xCoO₂, Li_xNiO₂ and λ-MnO₂ and Consequences for the Safety of Li-Ion Cells. *Solid State Ionics* **1994**, *69*, 265–270.
- (14) Yoon, W. S.; Chung, K. Y.; McBreen, J.; Yang, X. Q. A Comparative Study on Structural Changes of LiCo_{1/3}Ni_{1/3}Mn_{1/3}O₂ and LiNi_{0.8}Co_{0.15}Al_{0.05}O₂ during First Charge Using In Situ XRD. *Electrochem. Commun.* **2006**, *8*, 1257–1262.
- (15) Wu, L. J.; Nam, K. W.; Wang, X. J.; Zhou, Y. N.; Zheng, J. C.; Yang, X. Q.; Zhu, Y. M. Structural Origin of Overcharge-Induced Thermal Instability of Ni-Containing Layered-Cathodes for High-Energy-Density Lithium Batteries. *Chem. Mater.* **2011**, *23*, 3953–3960.
- (16) Kim, Y. Lithium Nickel Cobalt Manganese Oxide Synthesized Using Alkali Chloride Flux: Morphology and Performance as a

Cathode Material for Lithium Ion Batteries. *ACS Appl. Mater. Interfaces* **2012**, *4*, 2329–2333.

(17) Hwang, B. J.; Tsai, Y. W.; Carlier, D.; Ceder, G. A Combined Computational/Experimental Study on $\text{LiNi}_{1/3}\text{Co}_{1/3}\text{Mn}_{1/3}\text{O}_2$. *Chem. Mater.* **2003**, *15*, 3676–3682.

(18) Sun, Y. K.; Myung, S. T.; Park, B. C.; Prakash, J.; Belharouak, I.; Amine, K. High-Energy Cathode Material for Long-Life and Safe Lithium Batteries. *Nat. Mater.* **2009**, *8*, 320–324.

(19) Konishi, H.; Yuasa, T.; Yoshikawa, M. Thermal Stability of $\text{Li}_{1-y}\text{Ni}_x\text{Mn}_{(1-x)/2}\text{Co}_{(1-x)/2}\text{O}_2$ Layer-Structured Cathode Materials Used in Li-Ion Batteries. *J. Power Sources* **2011**, *196*, 6884–6888.

(20) Konishi, H.; Yoshikawa, M.; Hirano, T. The Effect of Thermal Stability for High-Ni-Content Layer-Structured Cathode Materials, $\text{LiNi}_{0.8}\text{Mn}_{0.1-x}\text{Co}_{0.1}\text{Mo}_x\text{O}_2$ ($x = 0, 0.02, 0.04$). *J. Power Sources* **2013**, *244*, 23–28.

(21) Bak, S. M.; Nam, K. W.; Chang, W.; Yu, X. Q.; Hu, E. Y.; Hwang, S.; Stach, E. A.; Kim, K. B.; Chung, K. Y.; Yang, X. Q. Correlating Structural Changes and Gas Evolution during the Thermal Decomposition of Charged $\text{Li}_x\text{Ni}_{0.8}\text{Co}_{0.15}\text{Al}_{0.05}\text{O}_2$ Cathode Materials. *Chem. Mater.* **2013**, *25*, 337–351.

(22) Toby, B. H. EXPGUI, A Graphical User Interface for GSAS. *J. Appl. Crystallogr.* **2001**, *34*, 210–213.

(23) Guilnard, M.; Croguennec, L.; Delmas, C. Thermal Stability of Lithium Nickel Oxide Derivatives. Part II: $\text{Li}_x\text{Ni}_{0.70}\text{Co}_{0.15}\text{Al}_{0.15}\text{O}_2$ and $\text{Li}_x\text{Ni}_{0.90}\text{Mn}_{0.10}\text{O}_2$ ($x = 0.50$ and 0.30). Comparison with $\text{Li}_x\text{Ni}_{1.02}\text{O}_2$ and $\text{Li}_x\text{Ni}_{0.89}\text{Al}_{0.16}\text{O}_2$. *Chem. Mater.* **2003**, *15*, 4484–4493.

(24) Guilnard, M.; Croguennec, L.; Denux, D.; Delmas, C. Thermal Stability of Lithium Nickel Oxide Derivatives. Part I: $\text{Li}_x\text{Ni}_{1.02}\text{O}_2$ and $\text{Li}_x\text{Ni}_{0.89}\text{Al}_{0.16}\text{O}_2$ ($x = 0.50$ and 0.30). *Chem. Mater.* **2003**, *15*, 4476–4483.

(25) Yoon, W. S.; Balasubramanian, M.; Yang, X. Q.; McBreen, J.; Hanson, J. Time-Resolved XRD Study on the Thermal Decomposition of $\text{Li}_{1-x}\text{Ni}_{0.8}\text{Co}_{0.15}\text{Al}_{0.05}\text{O}_2$ Cathode Materials for Li-ion Batteries. *Electrochem. Solid State Lett.* **2005**, *8*, A83–A86.

(26) Nam, K. W.; Yoon, W. S.; Yang, X. Q. Structural Changes and Thermal Stability of Charged $\text{LiNi}_{1/3}\text{Co}_{1/3}\text{Mn}_{1/3}\text{O}_2$ Cathode Material for Li-ion Batteries Studied by Time-Resolved XRD. *J. Power Sources* **2009**, *189*, 515–518.

(27) Nam, K. W.; Bak, S. M.; Hu, E. Y.; Yu, X. Q.; Zhou, Y. N.; Wang, X. J.; Wu, L. J.; Zhu, Y. M.; Chung, K. Y.; Yang, X. Q. Combining In Situ Synchrotron X-Ray Diffraction and Absorption Techniques with Transmission Electron Microscopy to Study the Origin of Thermal Instability in Overcharged Cathode Materials for Lithium-Ion Batteries. *Adv. Funct. Mater.* **2013**, *23*, 1047–1063.

(28) Cho, Y. H.; Jang, D.; Yoon, J.; Kim, H.; Ahn, T. K.; Nam, K. W.; Sung, Y. E.; Kim, W. S.; Lee, Y. S.; Yang, X. Q.; Yoon, W. S. Thermal Stability of Charged $\text{LiNi}_{0.5}\text{Co}_{0.2}\text{Mn}_{0.3}\text{O}_2$ Cathode for Li-ion Batteries Investigated by Synchrotron based In Situ X-ray Diffraction. *J. Alloys Compd.* **2013**, *562*, 219–223.

(29) Xiao, J.; Chernova, N. A.; Whittingham, M. S. Layered Mixed Transition Metal Oxide Cathodes with Reduced Cobalt Content for Lithium Ion Batteries. *Chem. Mater.* **2008**, *20*, 7454–7464.

(30) Shinova, E.; Stoyanova, R.; Zhecheva, E.; Ortiz, G. F.; Lavela, P.; Tirado, J. L. Cationic Distribution and Electrochemical Performance of $\text{LiCo}_{1/3}\text{Ni}_{1/3}\text{Mn}_{1/3}\text{O}_2$ Electrodes for Lithium-Ion Batteries. *Solid State Ionics* **2008**, *179*, 2198–2208.

(31) Yabuuchi, N.; Kim, Y. T.; Li, H. H.; Shao-Horn, Y. Thermal Instability of Cycled $\text{Li}_x\text{Ni}_{0.5}\text{Mn}_{0.5}\text{O}_2$ Electrodes: An In Situ Synchrotron X-ray Powder Diffraction Study. *Chem. Mater.* **2008**, *20*, 4936–4951.

(32) Wang, L.; Maxisch, T.; Ceder, G. A First-Principles Approach to Studying the Thermal Stability of Oxide Cathode Materials. *Chem. Mater.* **2007**, *19*, 543–552.

(33) Reed, J.; Ceder, G. Role of Electronic Structure in the Susceptibility of Metastable Transition-Metal Oxide Structures to Transformation. *Chem. Rev.* **2004**, *104*, 4513–4533.